Transition probabilities in neutron-rich ^{80,82}Se and the role of the $\nu g_{9/2}$ orbital

J. Litzinger,[1,*] A. Blazhev,[1] A. Dewald,[1] F. Didierjean,[2] G. Duchêne,[2] C. Fransen,[1] R. Lozeva,[3] D. Verney,[4] G. de Angelis,[5] D. Bazzacco,[6] B. Birkenbach,[1] S. Bottoni,[7] A. Bracco,[7] T. Braunroth,[1] B. Cederwall,[8] L. Corradi,[5] F. C. L. Crespi,[7] P. Désesquelles,[9] J. Eberth,[1] E. Ellinger,[1] E. Farnea,[6] E. Fioretto,[5] R. Gernhäuser,[10] A. Goasduff,[5] A. Görgen,[11,12] A. Gottardo,[5] J. Grebosz,[13] M. Hackstein,[1] H. Hess,[1] F. Ibrahim,[4] J. Jolie,[1] A. Jungclaus,[14] K. Kolos,[4] W. Korten,[11] S. Leoni,[7] S. Lunardi,[6] A. Maj,[13] R. Menegazzo,[15] D. Mengoni,[16,6] C. Michelagnoli,[6,17] T. Mijatovic,[18] B. Million,[19] O. Möller,[20] V. Modamio,[5] G. Montagnoli,[6] D. Montanari,[6] A. I. Morales,[7] D. R. Napoli,[5] M. Niikura,[4] N. Pietralla,[20] G. Pollarolo,[21] A. Pullia,[7] B. Quintana,[22] F. Recchia,[6] P. Reiter,[1] D. Rosso,[5] E. Sahin,[5] M. D. Salsac,[11] F. Scarlassara,[6] P.-A. Söderström,[20] A. M. Stefanini,[5] O. Stezowski,[23] S. Szilner,[18] Ch. Theisen,[11] J. J. Valiente-Dobón,[5] V. Vandone,[7] and A. Vogt[1]

[1]*Institut für Kernphysik, Universität zu Köln, D-50937 Köln, Germany*
[2]*Université de Strasbourg, CNRS, IPHC UMR 7178, F-67000 Strasbourg, France*
[3]*CSNSM, CNRS/IN2P3, Université Paris-Saclay, FR-91405 Orsay Campus, France*
[4]*Institut de Physique Nucléaire, CNRS/IN2P3 and Université Paris Sud, F-91405 Orsay, France*
[5]*Istituto Nazionale di Fisica Nucleare, Laboratori Nazionali di Legnaro, I-35020 Legnaro, Italy*
[6]*Istituto Nazionale di Fisica Nucleare, Sezione di Padova and Università di Padova, I-35131 Padova, Italy*
[7]*Dipartimento di Fisica, Università di Milano and INFN, Sezione di Milano, I-20133 Milano, Italy*
[8]*Department of Physics, Royal Institute of Technology, SE-10691 Stockholm, Sweden*
[9]*Centre de Spectrométrie Nucléaire et de Spectrométrie de Masse CSNSM, CNRS/IN2P3 and Université Paris-Sud, F-91405 Orsay Campus, France*
[10]*Physics Department E12, Technische Universität München, D-85748 Garching, Germany*
[11]*Institut de Recherche sur les lois Fondamentales de l'Univers - IRFU, CEA/DSM, Centre CEA de Saclay, F-91191 Gif-sur-Yvette Cedex, France*
[12]*Department of Physics, University of Oslo, P.O. Box 1048 Blindern, N-0316 Oslo, Norway*
[13]*The Henry Niewodniczański Institute of Nuclear Physics, Polish Academy of Sciences, ul. Radzikowskiego 152, 31-342 Kraków, Poland*
[14]*Instituto de Estructura de la Materia, CSIC, Madrid, E-28006 Madrid, Spain*
[15]*Istituto Nazionale di Fisica Nucleare, Sezione di Padova, I-35131 Padova, Italy*
[16]*Nuclear Physics Research Group, University of the West of Scotland, High Street, Paisley PA1 2BE, Scotland, United Kingdom*
[17]*GANIL, CEA/DSM-CNRS/IN2P3, BP 55027, 14076 Caen Cedex 5, France*
[18]*Ruder Bošković Institute, HR-10002 Zagreb, Croatia*
[19]*Istituto Nazionale di Fisica Nucleare, Sezione di Milano, I-20133 Milano, Italy*
[20]*Institut für Kernphysik, Technische Universität Darmstadt, D-64289 Darmstadt, Germany*
[21]*Dipartimento di Fisica Teorica dell' Università di Torino and INFN, I-10125 Torino, Italy*
[22]*Laboratorio de Radiaciones Ionizantes, Universidad de Salamanca, E-37008 Salamanca, Spain*
[23]*Université de Lyon, Université Lyon-1, IN2P3/CNRS, F-69622 Villeurbanne Cedex, France*

(Received 23 January 2018; published 27 April 2018)

Transition probabilities of intermediate-spin yrast and non-yrast excitations in ^{80,82}Se were investigated in a recoil distance Doppler-shift (RDDS) experiment performed at the Istituto Nazionale di Fisica Nucleare, Laboratori Nazionali di Legnaro. The Cologne Plunger device for deep inelastic scattering was used for the RDDS technique and was combined with the AGATA Demonstrator array for the γ-ray detection and coupled to the PRISMA magnetic spectrometer for an event-by-event particle identification. In ^{80}Se, the level lifetimes of the yrast (6_1^+) and (8_1^+) states and of a non-yrast band feeding the yrast 4_1^+ state are determined. A spin and parity assignment of the head of this sideband is discussed based on the experimental results and supported by large-scale shell-model calculations. In ^{82}Se, the level lifetimes of the yrast 6_1^+ state and the yrare 4_2^+ state and lifetime limits of the yrast (10_1^+) state and of the 5_1^- state are determined. Although the experimental results contain large uncertainties, they are interpreted with care in terms of large-scale shell-model calculations using the effective interactions JUN45 and jj44b. The excited states' wave functions are investigated and discussed with respect to the role of the neutron $g_{9/2}$ orbital.

DOI: 10.1103/PhysRevC.97.044323

I. INTRODUCTION

Selenium nuclei around the $N = 50$ shell closure are of particular interest for systematical nuclear-structure studies

*Corresponding author: jlitzinger@ikp.uni-koeln.de

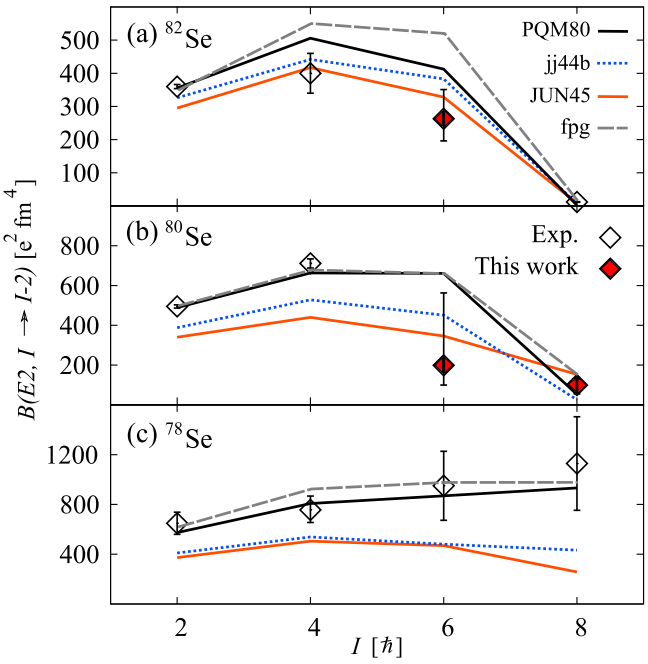

FIG. 1. Shell-model calculated $B(E2)$ values from previous works (from [14] labeled as PQM80 and from [12] labeled with jj44b, JUN45, and fpg) and experimental values of yrast states of $^{78-82}$Se. For a better overview and for the following discussion, experimental results from this work are already included in the figure and marked by the (red) filled symbols.

and have been investigated with great detail both theoretically and experimentally [1–18]. The level schemes of ^{80,82}Se were investigated and extended recently in multinucleon-transfer and fission experiments [3,9]. Information on transition probabilities for transitions between low-spin yrast states in ^{80,82}Se nuclei is available mainly from Coulomb-excitation experiments [6–8]. In addition, lifetimes of intermediate-spin yrast states are also of high importance for the understanding of nuclear structure.

In ^{82}Se, a sudden change in nuclear structure of the yrast band occurs at the isomeric 8_1^+ state. This is reflected by a small energy gap and a very small transition probability to the 6_1^+ state. Comparing excitation energies and $B(E2; 8_1^+ \rightarrow 6_1^+)$ values of the $N = 48$ isotonic chain, this effect culminates in $^{82}_{34}$Se$_{48}$ [16]. In Fig. 1, $B(E2; I \rightarrow I-2)$ values for the yrast band up to 8_1^+ are depicted for ^{78,80,82}Se. In ^{78}Se, experimental $B(E2; I \rightarrow I-2)$ values increase up to $I = 8$ with no indication of a structural change. This is in clear contrast to ^{82}Se with its very small $B(E2; 8_1^+ \rightarrow 6_1^+) = 11.9(6)\ e^2\text{fm}^4$ [16]. The $B(E2)$ values of transitions from the 6_1^+ state in ^{82}Se and decays of the (6_1^+) and (8_1^+) states in ^{80}Se were unknown prior to this work. Thus, it was unclear how the transition of collectivity along the yrast bands in ^{80,82}Se proceeds and how this develops along the selenium isotopic chain when approaching $N = 50$. In Ref. [14,15], this topic was addressed by using a phenomenological monopole and quadrupole pairing plus quadrupole-quadrupole interaction for the mass region 80. In addition, full shell-model and pair-truncated shell-model (PTSM) calculations were performed (see also Fig. 1), in which the corresponding $B(E2)$ strengths are labeled with PQM80. The PTSM predicts that a pair of fully aligned $g_{9/2}$ neutrons is essential for the description of states with spin $I \gtrsim 8^+$ for ^{80,82}Se, while lowest yrast states up to the 6_1^+ state in ^{80,82}Se are ascribed to rotational and vibrational collective motions [15].

For the selenium isotopic chain starting from ^{78}Se up to the semimagic nucleus ^{84}Se, shell-model calculations using the effective interactions JUN45 [19], jj44b [20,21], and fpg [22] with ^{56}Ni and ^{48}Ca as inert cores were reported in Ref. [12]; the resulting $B(E2)$ values are plotted in Fig. 1. The general behavior of $B(E2)$ strengths in ^{78,80,82}Se is similar in the presented shell-model calculations. The values calculated by fpg and PQM80 describe the previously known experimental data very well with the exception of the $4_1^+ \rightarrow 2_1^+$ transition in ^{82}Se. The influence of the missing $f_{7/2}$ shell in the model space of JUN45 and jj44b calculated values results in lower $B(E2)$ values compared to PQM80 and fpg, especially for ^{78}Se. Besides this, there are slight differences in the $B(E2)$ trend for the 6^+ and 8^+ states in ^{80}Se between jj44b, JUN45, and fpg, which calls for experimental clarification.

Further on, yrare states provide an additional testing ground for the discussed theoretical descriptions. In ^{80}Se and ^{82}Se, lowest yrare states have similar excitation energies and show an equal decay behavior [cf. Figs. 2(a) and 2(b)]. Prior to this work, lifetimes of yrare 2_2^+ states in ^{80,82}Se were measured [7]. The lifetime of the 4_2^+ yrare state in ^{80}Se was deduced from a Doppler-shif attenuation method (DSAM) experiment [17], while the 4_2^+ lifetime in ^{82}Se was unknown prior to this work.

In ^{80}Se, a sideband on top of the yrast 4_1^+ state was observed for the first time by the authors of Ref. [5] (see Fig. 2). However, a spin and parity assignment could not be provided. This will be addressed in this work based on experimental data and shell-model calculations.

This paper is structured as follows: the experimental setup is introduced and the analysis procedure is explained in detail (Sec. II). The lifetime analysis is presented for each nucleus (Sec. III). The paper closes with the discussion of the experimental results particularly with regard to large-scale shell-model calculations (Sec. IV).

II. EXPERIMENTAL DETAILS AND LIFETIME ANALYSIS PROCEDURE

A recoil distance Doppler-shift (RDDS) experiment was performed at the Istituto Nazionale di Fisica Nucleare (INFN) Laboratori Nazionali di Legnaro (LNL), Legnaro, Italy. ^{80}Se nuclei were produced via a $-2n$ multinucleon-transfer reaction induced by a ^{82}Se beam provided by the Tandem-XTU and the ALPI superconducting LINAC accelerator at an energy of 577 MeV. The beam impinged onto a ^{238}U plunger target with a thickness of 2 mg/cm^2 which was evaporated onto a 1.2 mg/cm^2 Ta backing facing the beam mounted in the Cologne Plunger device for deep-inelastic reactions [24]. ^{82}Se nuclei were mainly excited via multistep Coulomb excitation. A ^{93}Nb degrader foil with a thickness of 4.1 mg/cm^2 was mounted downstream from the target. Projectile-like recoils were therefore slowed down before entering the PRISMA magnetic spectrometer [25–28] for the event-by-event particle

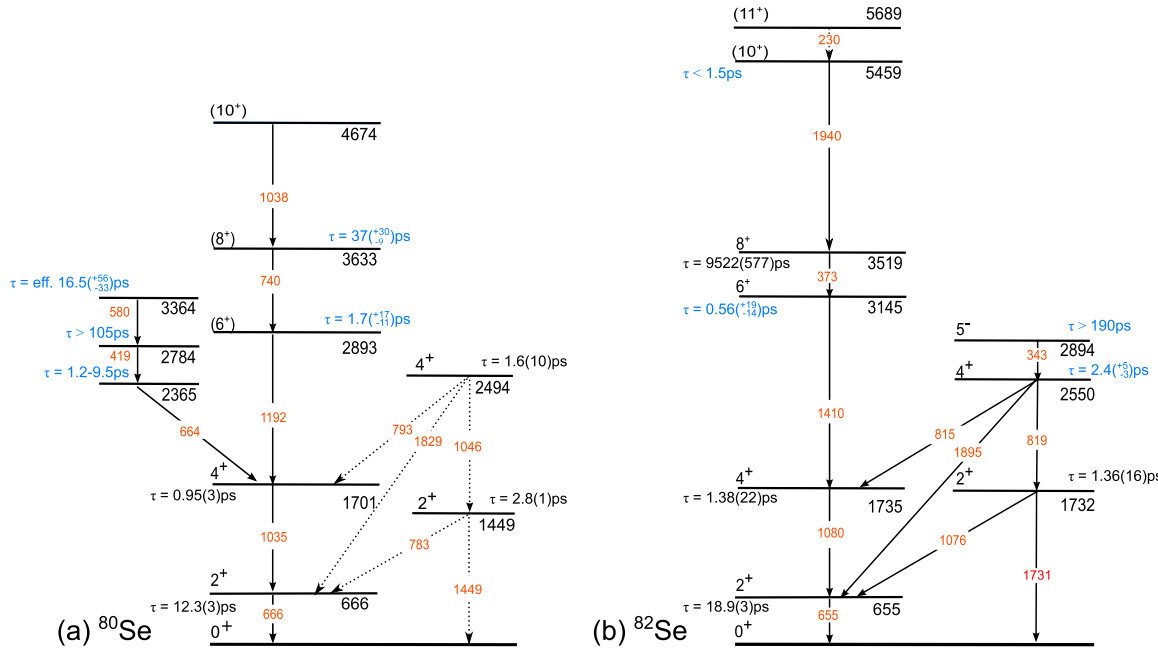

FIG. 2. Partial level schemes of ^{80,82}Se including level lifetimes from this work and from NNDC [23]. New lifetime information (lifetimes, effective lifetimes, or lifetime limits) deduced from this work is written in blue (gray). Dotted transitions in ^{80}Se are not visible in the γ-ray spectra presented in this work and are included for comparison with ^{82}Se. Excitation energies and γ-ray energies are given in keV, taken from NNDC [23] and Ref. [5]. Further details are given in the text.

identification. Three target-to-degrader distances were measured. The AGATA spectrometer in its demonstrator configuration [29,30] was used to detect the γ rays of the deexciting reaction products.

A pulse-shape analysis yields the interaction position of γ rays inside the detector [31]. From this, γ-ray energies and their first interaction points are reconstructed using the Orsay forward-tracking algorithm [32]. Angular information deduced from the first γ-ray interaction point and the momentum vector provided by PRISMA are used for the Doppler correction. The total kinetic energy loss (TKEL) of the recoils is reconstructed event by event using relativistic two-body reaction kinematics [27,28,33], assuming a binary reaction and imposing the conservation of linear momentum.

A detailed discussion of the experimental details including the mass resolution for $Z = 34$ is given in Ref. [11].

The decay curve of an excited state is the intensity ratio of the degraded I_D and the fast peaks I_T with respect to the distance x between the foils, $R(x) = I_D(x)/[I_D(x) + I_T(x)]$. To determine lifetimes from RDDS data, the solution of the corresponding system of differential equations, the Bateman equations, is fitted to the decay curve [24]. In this case, exact distance information is crucial. The plunger device provides relative distances with a precision of typically <0.1 μm for small distances, but with an uncertain offset. This offset is fitted to three decay curves of transitions from levels in ^{82}Se with well-known lifetimes from prior Coulomb excitation and DSAM experiments [6,7,34]. The three target-to-degrader distances in this experiment are 38(1), 257(2), and 507(7) μm with a zero-point uncertainty of 4 μm.

In Ref. [11], a method to determine lifetimes from RDDS data using summed γ-ray spectra of different target-to-degrader distances was introduced. This can be used if statistics are insufficient to determine peak intensities for each distance individually. In this case, the lifetime is calculated from the solution of the differential Bateman equations as follows:

$$R_{\mathrm{sum}} = \frac{\sum_{j=1}^{n} I_{Dj}}{\sum_{j=1}^{n} I_{Dj} + \sum_{j=1}^{n} I_{Tj}} = \sum_{j=1}^{n} n_j R(x_j), \qquad (1)$$

where I_{Dj} (I_{Tj}) denotes the peak area of the transition of interest from emission before (after) passing the degrader for each target-to-degrader distance x_j, $R(x_j)$ is the decay curve, described by the solution of the Bateman equations, and n_j denotes normalization factors for each distance. This method is used for the lifetime determination in several cases described in this work.

A Monte Carlo simulation is used to determine lifetimes and related errors. Uncertainties from the intensity ratios of feeding transitions and of the transitions of interest as well as uncertainties from absolute distance values and from transition intensities are taken into account. Expectation values of the generated distributions correspond to the level lifetimes; errors are deduced from the 1σ quantiles of the probability distributions in both directions.

Recoil velocities are in the range of $\beta \approx 9\%$. Therefore, relativistic effects are taken into account. Detector efficiencies are calculated using the GEANT4 toolkit [35], evaluated with experimental data. Different detector efficiencies of the fast and degraded components of each transition are considered.

Due to low statistics, a $\gamma\gamma$-coincidence analysis is not feasible. In case of a γ-ray analysis in singles, all observed feeders are taken into account with their experimentally observed intensities. Besides, one has to deal with the possibility of

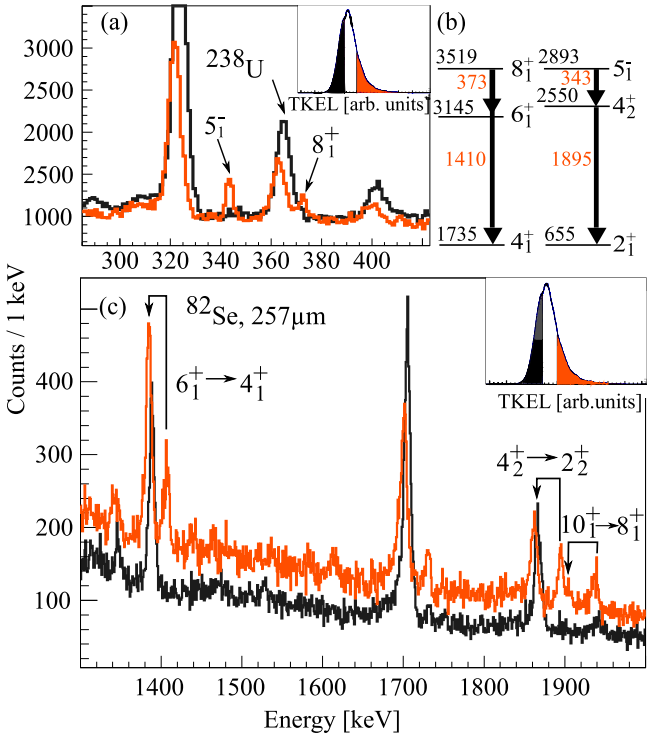

FIG. 3. TKEL-gated γ-ray spectra for ^{82}Se. Inset: TKEL distribution for ^{82}Se showing TKEL gates which are under comparison. All γ-ray spectra are from the same target-to-degrader distance (257 μm). Further details are given in the text.

unknown feeding transitions, so-called side-feeding. Feeding transitions from levels with lifetimes in the range of that of the level of interest or larger influence the time behavior of the level of interest. Therefore, those are relevant for the lifetime analysis.

The lifetime analysis presented in this work benefits from the possibility to select nuclei with specific total kinetic energy losses (TKEL). The TKEL is given by

$$\begin{aligned} \mathrm{TKEL} &= -Q = -(m_T + m_B - m_{TL} - m_{BL})c^2 \\ &= E_{TL} + E_{BL} - E_T - E_B \end{aligned} \quad (2)$$

where m_T denotes the mass of the target nucleus and m_B the mass of the beam nucleus; m_{TL} denotes the targetlike and m_{BL} the beamlike reaction products. The underlying formula and assumptions are explained in more detail in Ref. [33]. In the actual case, the kinetic energy of the beamlike particles E_{BL} was measured directly with the PRISMA spectrometer; the energy of the target $E_T = 0$ MeV and the energy of the beam E_B is known. E_{TL} can be calculated by measuring the angle of emission of beam-like particles, θ_B, with respect to the original direction of the beam.

The effect of different TKEL conditions on ^{82}Se gated γ-ray spectra is visible in Fig. 3. By choosing different gates for the TKEL, higher-lying states can be suppressed or enhanced; see also Ref. [27]. This effect is clearly visible in Fig. 3(a). For a gate on large TKEL values (red or light gray) the 5^-_1 and 8^+_1 states are clearly visible, whereas for a gate on low TKEL values (black) both states are completely suppressed. This allows

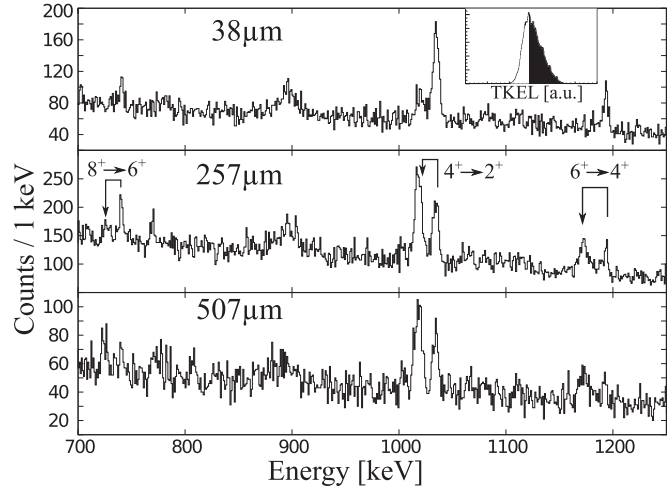

FIG. 4. γ-ray spectra of ^{80}Se centered at the energy of the yrast $4^+_1 \rightarrow 2^+_1$ transition for three different target-to-degrader distances, plotted on top of each other. More details are given in the text.

us to construct γ-ray spectra with different feeding patterns for energetically lower states [36,37]. As a consequence, the experimentally observed time behavior (decay curve) of those transitions is clearly affected; see Fig. 3(c) for the $6^+_1 \rightarrow 4^+_1$ and $4^+_2 \rightarrow 2^+_2$ transitions. Both 8^+_1 and 5^-_1 states have long lifetimes compared to the flight time of the recoils between the target and degrader foils. The effect of these long-living states can be seen in transitions from the 6^+_1 and 4^+_2 states; see Fig. 3(c). In both cases, despite their short lifetimes, a clear degrader component I_D is visible due to the slow feeding [cf. Fig. 3(b)]. This allows to cross-check the lifetime analysis by using different feeding patterns.

An additional advantage is given in the improved peak-to-background ratio by choosing suitable TKEL gates. Background from random coincidences, mainly from fission-like reaction products, can be reduced by a gate on the low region of the TKEL distribution; cf. Fig. 3 and Refs. [38,39].

III. LIFETIME ANALYSIS

A. ^{80}Se

1. Yrast states

Figure 4 shows partial γ-ray spectra of ^{80}Se centered around the energy of the $4^+_1 \rightarrow 2^+_1$ transition for the three target-to-degrader distances. The TKEL gate, indicated by the inset, is used to improve the peak-to-background ratio especially for high-lying states. As the (8^+_1) state is a direct feeder of the (6^+_1) state, its lifetime analysis is crucial for the analysis of the (6^+_1) state and is discussed first.

The lifetime of the (8^+_1) state is relatively long compared to the recoil flight times regarded in this experiment, thus only a small flight component occurs; see Fig. 4. The only feeding transition described before is a transition from the (10^+_1) state with $E_\gamma = 1038$ keV. As the 4^+_1 state decays with a similar transition energy of $E_\gamma = 1035$ keV a significant contribution to the peak intensity cannot be ruled out *a priori*. Nevertheless, a level lifetime of $\approx$1–2 ps is expected for the 10^+_1 state by

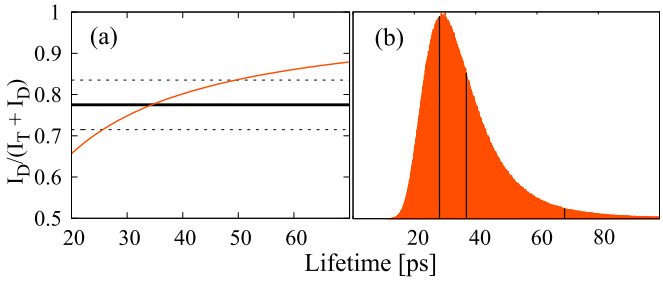

FIG. 5. $R(\tau)$ curve (a) and error estimation (b) for the $(8_1^+) \rightarrow (6_1^+)$ transition in ^{80}Se. The mean value and 1σ quantiles are marked. A lifetime of $\tau = 37(^{+31}_{-9})$ ps is determined. More details are given in the text.

comparison with neighboring nuclei ^{82,84}Kr, and, following shell-model calculations, it can be assumed that the (10_1^+) state decays much faster than the (8_1^+) state. Therefore, its influence on the (8_1^+) state time behavior can be neglected within the accuracy achieved here.

The intensity ratio obtained in this work of the $(8_1^+) \rightarrow (6_1^+)$ transition from the summed spectra [Eq. (1)] is $R_{\rm sum} = 0.78(7)$ and is marked in Fig. 5(a). The statistics of the different target-to-degrader distances are normalized using the number of nuclei in the PRISMA particle gate n_j for each distance j. The resulting $R(\tau)$ curve is shown in Fig. 5(a), the lifetime distribution resulting from the Monte Carlo simulation is depicted in Fig. 5(b). The lifetime of the (8_1^+) state is determined to be $\tau = 37(^{+31}_{-9})$ ps.

For the (6_1^+) state, the evolution of the flight and degraded components with respect to the flight time between the target and the degrader foil is clearly visible; see Fig. 4. The (8_1^+) state is populated with 47(7)% relative to the (6_1^+) state. The influence of slow feeding from the (8_1^+) state to the $(6_1^+) \rightarrow 4_1^+$ time behavior is clearly visible in the decay curve in the time-of-flight segment from 10–20 ps (see Fig. 6). Because of poor statistics, intensity ratios have large uncertainties of up to 8%. In addition, the intensity of the (8_1^+) state as well as its lifetime have large error bars. As a consequence, the simulation using a normal Bateman fit and the intensity ratio of each target-to-degrader distance do not lead to a clear lifetime distribution; see Fig. 6(b). Mean value and 1σ quantiles lead to a lifetime of $\tau = 3.7(^{+37}_{-16})$ ps. Using summed γ-ray spectra, the intensity ratio of the fast and degraded components for the (6_1^+) state is 0.43(3). The resulting probability distribution is depicted in Fig. 6(c), leading to a lifetime of $\tau = 1.7(^{+17}_{-11})$ ps.

2. Non-yrast states

Transitions from a non-yrast band feeding the first 4_1^+ state are visible in the γ-ray spectra; those are already described in Ref. [5]. The fact that only a degraded component of the Doppler-shifted 419-keV transition depopulating the excited state at 2784 keV is observed in our data for all distances leads to a lower lifetime limit of $\tau \geqslant 105$ ps.

A flight-time-dependent component development is visible for the transition from a level at $E^x = 3364$ keV decaying via $E_\gamma = 580$ keV. From summed γ-ray spectra an effective

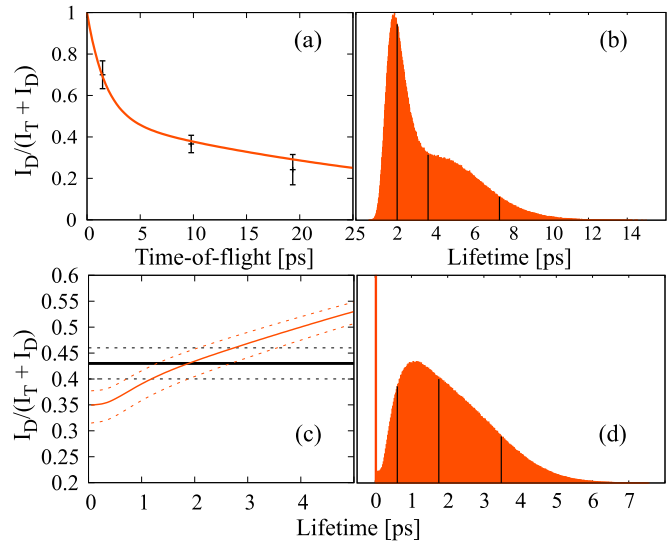

FIG. 6. Decay curve (a) with error estimation (b) and $R(\tau)$ curve (c) with error estimation (d) for the $(6_1^+) \rightarrow 4_1^+$ transition in ^{80}Se. A lifetime of $\tau = 1.7(^{+17}_{-11})$ ps is determined. More details are given in the text.

lifetime of $\tau = 16.5(^{+56}_{-33})$ ps is derived. No information about feeding is known from previous experiments, therefore an effective lifetime is given in this case.

Due to the limits of the detector resolution, a transition with $E_\gamma = 664$ keV feeding the yrast 4_1^+ state from a state at $E^* = 2365$ keV and the $2_1^+ \rightarrow 0_1^+$ transition with $E_\gamma = 666$ keV are not separated. The influence of this transition on transitions from the yrast 4_1^+ and 2_1^+ states is clearly visible in the decay curves of these states. Lifetimes of the 2_1^+ and 4_1^+ state are known from Refs. [7,8]. The lifetime of the 2365-keV level is unknown. Furthermore, the intensity of this transition relative to the $2_1^+ \rightarrow 0_1^+$ transition cannot be measured, too. As two experimental decay curves are available, one from the $4_1^+ \rightarrow 2_1^+$ transition and one from the doublet of the 664-keV transition and the $2_1^+ \rightarrow 0_1^+$ transition, both lifetime and feeding intensity of the 2365-keV level can be obtained by a simultaneous fit minimizing the summed χ^2. From the simulation, an intensity of $I_{664} = 25(^{+6}_{-5})\%$ relative to the intensity of the $2_1^+ \rightarrow 0_1^+$ transition results; see Fig. 7(c). As experimental uncertainties are large, the resulting lifetime distribution from the Monte Carlo simulation points to two lifetime maxima with different weighting; see Fig. 7(b). The first maximum points to a level lifetime of about 1.7(5) ps with 13% weighting. It results from the scenario that intensity ratios of both decay curves are shifted to lowest values compatible with the errors. The second maximum points to a level lifetime of 6.4(31) ps with 87% weighting. In the further discussion, the extreme limits of both lifetimes, and no expectation values, are used. A lifetime range of 1.2–9.5 ps results for the 2365-keV level.

B. ^{82}Se

1. The yrast 6_1^+ state

The yrast 6_1^+ state of ^{82}Se exhibits a very short lifetime compared to the flight time of the two larger target-to-degrader

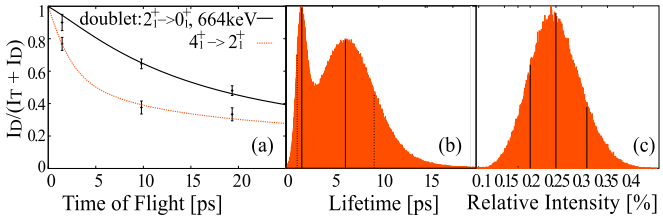

FIG. 7. Decay curves (a), lifetime distribution (b), and intensity probability distribution (c) for the transition from a level with $E^* = 2365$ keV. The lifetime and the decay intensity are derived by a simultaneous fit minimizing the summed χ^2 of Bateman fits for decay curves from a doublet of the decay of a level with $E^* = 2365$ keV with the $2_1^+ \to 0_1^+$ transition (black, solid) and from the $4_1^+ \to 2_1^+$ transition (red, dotted), using lifetime information from previous experiments. More details are given in the text.

distances. Only for the smallest foil distance is a degrader component visible, aside from the constant part which arises from slow level feeding from the yrast 8_1^+ state; see Fig. 8. In the case of small level lifetimes, the slowing-down time in the degrader has to be considered. Nuclei which decay while passing the degrader foil are slowed down less than those which decay after passing the whole degrader foil. Therefore, in the γ-ray spectra events occur between the fast and degraded components and in the fast component, which are part of I_D. For the analysis presented in this work, this effect is relatively small, as nuclei only spent about 0.2 ps in the degrader foil before leaving towards the PRISMA spectrometer. But in the case of several transitions in ^{82}Se, small errors, of $\leqslant$2%, of intensity ratios of fast and degraded components

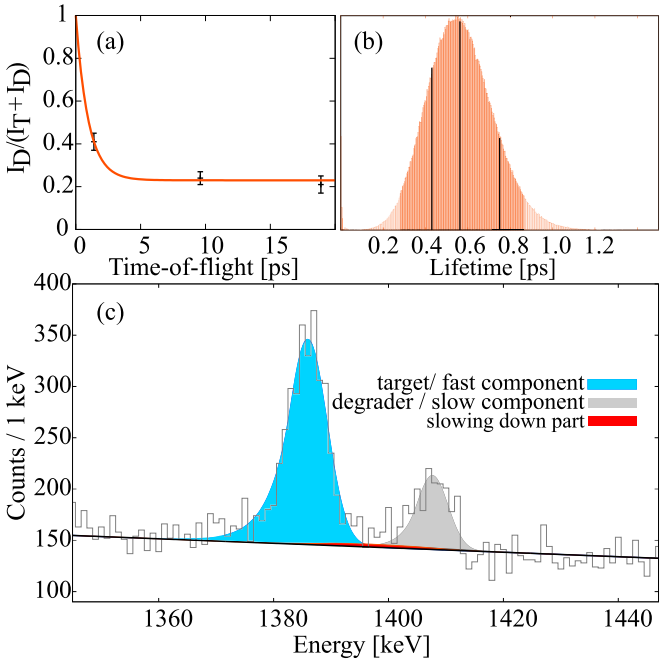

FIG. 8. Decay curve (a) and error estimation (b) for the $6_1^+ \to 4_1^+$ transition in ^{82}Se. A lifetime of $\tau = 0.56(^{+19}_{-14})$ ps is determined. (c) Slowing-down process for the $6_1^+ \to 4_1^+$ transition in ^{82}Se. More details are given in the text.

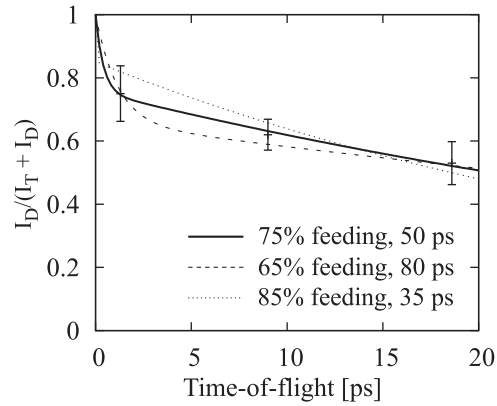

FIG. 9. Decay curve for the 1940-keV transition $(10_1^+) \to 8_1^+$ in ^{82}Se using the feeding hypothesis described in the text. The solid line shows the best fit within the errors, dashed and dotted lines depict extreme feeding scenarios assuming 85% and 65% feeding with 35 and 80 ps, respectively. More details are given in the text.

can be achieved, thus in these cases even small effects have to be considered. The amount of wrongly assigned events is estimated simulating the slowing-down progress, dividing the degrader foil into ten parts. The energy loss in each of these segments is calculated using the program LISE++ [40] with the Atima 1.2 logarithms and corrected by 3%, as LISE++ underestimates the energy loss by this amount, evaluated by comparing with the Doppler shift.

This results in a lifetime of $\tau = 0.56(^{+19}_{-14})$ ps for the yrast 6_1^+ state in ^{82}Se.

2. The yrast (10_1^+) state

In Refs. [5,9], the yrast $(10_1^+) \to 8_1^+$ transition with $E_\gamma = 1940$ keV was discussed. In addition, a 5689-keV level feeding the yrast (10_1^+) state ($E_\gamma = 230$ keV) was found and proposed as the (11^+) state. Unfortunately, the $(11^+) \to (10_1^+)$ transition is hidden in the ^{238}U background, Doppler corrected for the velocities of $A \approx 80$ ejectiles. Flight and degraded components of the $(10_1^+) \to 8_1^+$ transition are clearly visible in TKEL-gated ^{82}Se γ-ray spectra; see Fig. 3(c). The corresponding decay curve is depicted in Fig. 9 and can only be described assuming a slow feeder with high intensity. The best description of the observed decay curve is given by assuming 75% feeding from a level with 50 ps lifetime, depicted with a solid line in Fig. 9. The resulting lifetime is 0.4 ps. Within the errors, the decay curve can be described assuming 85% and 65% feeding with 35 and 80 ps, respectively, depicted in Fig. 9 with dashed and dotted lines. In all described cases, the resulting lifetime of the (10_1^+) state is smaller than 1 ps, and an upper lifetime limit of $\tau \leqslant 1.5$ ps can be given.

3. Non-yrast states

From the 4_2^+ state, three depopulating branches are identified. This state decays to the first 2_1^+ state via $E_\gamma = 1895.5$ keV and to the 4_1^+ and 2_2^+ states via $E_\gamma = 815.1$ keV and $E_\gamma = 818.6$ keV, respectively. The latter two γ-ray decays are too close in energy to be distinguished, therefore the decay to

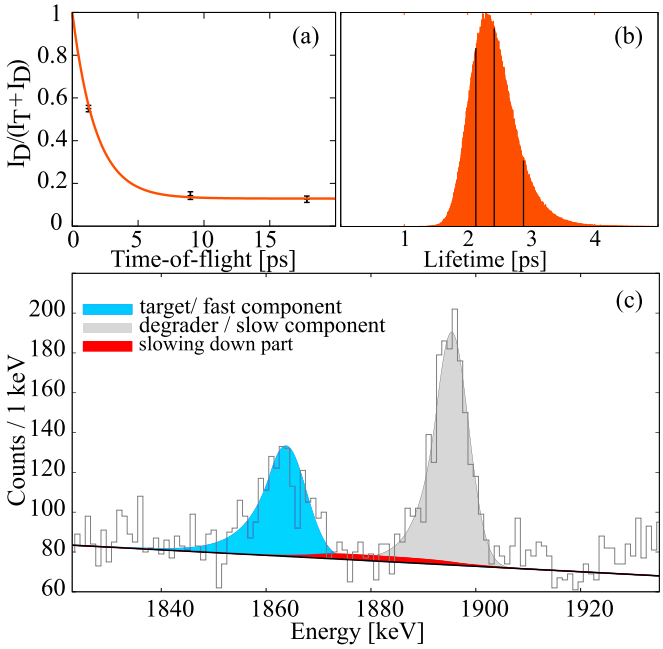

FIG. 10. Decay curve (a) and error estimation (b) for the $4_2^+ \rightarrow 2_1^+$ transition in ^{82}Se. A lifetime of $\tau_{4_2^+} = 2.4(^{+5}_{-3})$ ps is determined. (c) Slowing-down process for the $4_2^+ \rightarrow 2_1^+$ transition in ^{82}Se. More details are given in the text.

the first 2_1^+ state is analyzed; see Fig. 10. The only observed feeding transition arises from a long-living 5^- state. The aforementioned slowing-down effect is slightly stronger than in the case of the 6_1^+ decay because the smallest target-to-degrader distance lies exactly in the sensitive range of the level lifetime. A lifetime of $\tau = 2.4(^{+5}_{-3})$ ps results for the yrare 4_2^+ state in ^{82}Se.

In the case of the 5^- state only the degraded component occurs in the γ-ray spectra. This is consistent with the $4_2^+ \rightarrow 2_1^+$ transition for which no target and degrader component development between the second and third distance is observed; see Fig. 10. A lower lifetime limit of $\tau_{5^-} \geqslant 190$ ps can be given.

In Table I, the new lifetimes for ^{80,82}Se derived from this work are summarized.

IV. DISCUSSION

As shown in Fig. 2, the nuclei ^{80,82}Se show similar level schemes, and the 2_1^+ and 4_1^+ yrast states have comparable

TABLE I. Summary of new lifetime information derived in this work.

^{80}Se		^{82}Se	
J^π	$\tau(J^\pi)$ (ps)	J^π	$\tau(J^\pi)$ (ps)
(6_1^+)	$1.7(^{+17}_{-11})$	6_1^+	$0.56(^{+19}_{-14})$
(8_1^+)	$37(^{+30}_{-9})$	(10_1^+)	$\leqslant 1.5$
$E^* = 2365$ keV	1.2–9.5	4_2^+	$2.4(^{+5}_{-3})$
$E^* = 2785$ keV	$\geqslant 105$	5_1^-	$\geqslant 190$
$E^* = 3364$ keV	eff. $16.5(^{+56}_{-33})$		

excitation energies within a few keV. The structural change at the 8^+ state, reflected by a small $8^+ \rightarrow 6^+$ transition energy, is clearly more pronounced in ^{82}Se compared to ^{80}Se. The known $B(E2; 8^+ \rightarrow 6^+)$ in ^{82}Se also supports this difference in structure. Our experimental results completed the $B(E2)$ data of the yrast bands in these nuclei up to the 8^+ state.

In contrast to ^{78}Se, the $B(E2; 6^+ \rightarrow 4^+)$ values for both ^{80,82}Se show a reduction of $E2$ strengths compared to the corresponding $4^+ \rightarrow 2^+$ transition strengths (cf. Table II and Fig. 1). The $B(E2; I \rightarrow I-2)$ values continuously decrease from $I = 4$ to $I = 8$ for ^{80}Se, showing a behavior similar to ^{82}Se and confirming the theoretical predictions [12,14,15] (see Fig. 1 and Table II). The decrease factor from $I = 4$ to $I = 8$ is 34 for ^{82}Se, but only 7 in the case of ^{80}Se. This reduction of collectivity towards the 8^+ state is more sudden in ^{82}Se than in ^{80}Se. In order to address these differences, the experimental results are compared to shell-model calculations, focusing on the role of the $\nu g_{9/2}$ orbital and differences in the wave functions of the 6_1^+ and 8_1^+ states.

A. Shell-model calculations for ^{80,82}Se

Shell-model calculations for ^{80,82}Se are performed using ^{56}Ni as an inert core in the $f_{5/2}pg_{9/2}$ valence space using the JUN45 [19] and jj44b [20] effective interactions and the code NuShellX@MSU [41]. Standard effective charges, $e_\pi = 1.5e$ and $e_\nu = 0.5e$ for protons and neutrons, respectively, are used for calculating reduced $E2$ strengths. On the one hand, this was done to have a direct comparison with the truncated fpg calculations from Ref. [12], which are shown in Fig. 1 and which also used standard effective charges. On the other hand, these effective charges give an optimal description of both low and intermediate spin yrast transitions in ^{80,82}Se. Although the suggested effective charges of $e_\pi = 1.5e$ and $e_\nu = 1.1e$ [19] reproduce the yrast $B(E2; 2^+ \rightarrow 0^+)$ values and the known quadrupole moments in the region better, they overestimate most $B(E2; I \rightarrow I-2)$ values for the intermediate yrast states in ^{80,82}Se. For the sake of completeness, we note that the PQM80 calculations [14,15], shown in Fig. 1, use effective charges of $e_\pi = 1.65e$ and $e_\nu = 0.65e$. Magnetic transition strengths presented in this work (see Table II) are calculated using effective nucleon g factors $g_{s,\text{eff}} = 0.7 \times g_{s,\text{free}}$, as suggested in Ref. [19].

In addition to Table II, experimental and calculated excitation energies and $B(E2)$ values for yrast states in ^{80}Se and ^{82}Se up to the $10_1^+ \rightarrow 8_1^+$ transition and excitation energies of lowest yrare levels and selected negative-parity states are also depicted in Fig. 11. New experimental $B(E2)$ values from this work are marked red (gray). Although shell-model calculations using the JUN45 and jj44b interaction with detailed information on excitation energies and the $B(E2)$ values up to the $8_1^+ \rightarrow 6_1^+$ transition were already published and discussed in Ref. [12], additional information on $B(E2)$ values of higher yrast and lowest yrare states as well as spin couplings and wave function information is given and discussed in the following.

1. *Yrast states of* ^{80,82}Se

As already discussed in Ref. [12], the energies of the yrast bands are well reproduced by JUN45 and jj44b. The

TABLE II. Summary of the experimental results for ^{80,82}Se compared to large-scale shell-model calculations. Italics indicate prior results. Experimental γ-transition energies are taken from NNDC database [23] and from Ref. [5]. In all cases, transition probabilities are calculated from lifetimes, transition energies, branching ratios, and multipole mixing ratios given in the table. In cases where experimental multipole mixing ratios are missing or type and multipolarity of the transition are unclear transition probabilities are calculated assuming the extreme limits of pure $E2$, $E1$, $M2$, or $M1$ transitions, respectively, marked with *. Effective charges of $e_\pi = 1.5e$, $e_\nu = 0.5e$, and effective nucleon g factors $g_{s,\mathrm{eff}} = 0.7 \times g_{s,\mathrm{free}}$ are used. See text for further details.

A	$J^{\pi 2} \to J^{\pi 1}$	Branching	E_γ (keV)	Multipolarity, δ	Experiment: this work/*previous work*		Theory	
					$\tau(J^{\pi 2})$ (ps)	$B(\sigma\lambda; J^{\pi 2} \to J^{\pi 1})$	JUN45 $B(\sigma\lambda)$	jj44b $B(\sigma\lambda)$
^{80}Se	$2_1^+ \to 0_1^+$		666.15(10)	$E2$	*12.3(3)* [8]	*506(12)* $e^2\mathrm{fm}^4$	340 $e^2\mathrm{fm}^4$	388 $e^2\mathrm{fm}^4$
	$4_1^+ \to 2_1^+$		1035.1(1)	$E2$	*0.95(3)* [7]	*720(20)* $e^2\mathrm{fm}^4$	440 $e^2\mathrm{fm}^4$	528 $e^2\mathrm{fm}^4$
	$(6_1^+) \to 4_1^+$		1194	$E2$	$1.7(^{+17}_{-11})$	$2.0(^{+3.6}_{-1.0}) \times 10^2$ $e^2\mathrm{fm}^4$	346 $e^2\mathrm{fm}^4$	451 $e^2\mathrm{fm}^4$
	$(8_1^+) \to (6_1^+)$		740	$E2$	$37(^{+30}_{-9})$	$100(^{+32}_{-45})$ $e^2\mathrm{fm}^4$	153 $e^2\mathrm{fm}^4$	26 $e^2\mathrm{fm}^4$
	$(10_1^+) \to (8_1^+)$		1080	$E2$			284 $e^2\mathrm{fm}^4$	269 $e^2\mathrm{fm}^4$
	$2_2^+ \to 0_1^+$	100(3)	1449.4(1)	$E2$	*2.8(1)* [7]	*27(2)* $e^2\mathrm{fm}^4$	4.5 $e^2\mathrm{fm}^4$	3.5 $e^2\mathrm{fm}^4$
	$\to 2_1^+$	66.6(10)	783.1(1)	$M1, \delta = -5^{+2}_{-6}$		$7(^{+4}_{-7}) \times 10^{-4}$ μ_N^2	0.04 μ_N^2	0.02 μ_N^2
				$E2$		$3.8(^{+6.6}_{-2.1}) \times 10^2$ $e^2\mathrm{fm}^4$	185 $e^2\mathrm{fm}^4$	106 $e^2\mathrm{fm}^4$
	$4_2^+ \to 2_1^+$	53(5)	1828.8(3)	$E2$	*1.6(10)* [17]	$9(^{+23}_{-6})$ $e^2\mathrm{fm}^4$	2.4 $e^2\mathrm{fm}^4$	5.1 $e^2\mathrm{fm}^4$
	$\to 2_2^+$	≈3	1046 ?	$E2$		≈8	126 $e^2\mathrm{fm}^4$	212 $e^2\mathrm{fm}^4$
	$\to 4_1^+$	100(30)	793.0(3)	$M1, \delta = 1.1(1)$		$0.02(^{+3}_{-1})$ μ_N^2	0.03 μ_N^2	0.08 μ_N^2
				$E2$		$5.7(^{+9.5}_{-2.3}) \times 10^2$ $e^2\mathrm{fm}^4$	0.02 $e^2\mathrm{fm}^4$	57 $e^2\mathrm{fm}^4$
	$E^x = 2365 \to 4_1^+$		664	$E2^*$	1.2–9.5	668–5292 $e^2\mathrm{fm}^4$		
				$E1^*$		$(0.23\text{–}1.8) \times 10^{-3}$ $e^2\mathrm{fm}^2$		
				$M2^*$		$(6.0\text{–}47.8) \times 10^4$ $\mu_N^2\mathrm{fm}^2$		
				$M1^*$		0.02–0.16 μ_N^2		
	$E^x = 2784 \to E^x = 2365$		419	$E2^*$	$\geqslant 105$	$\leqslant 605$ $e^2\mathrm{fm}^4$		
				$E1^*$		$\leqslant 0.7 \times 10^4$ $e^2\mathrm{fm}^2$		
				$M2^*$		$\leqslant 5.5 \times 10^4 \mu_N^2\mathrm{fm}^2$		
				$M1^*$		$\leqslant 0.007$ μ_N^2		
	$E^x = 3364 \to E^x = 2784$		580	$E2^*$	eff. $16.5(^{+56}_{-33})$	$\geqslant 565$ $e^2\mathrm{fm}^4$		
				$E1^*$		$\geqslant 1.5 \times 10^{-4}$ $e^2\mathrm{fm}^2$		
				$M2^*$		$\geqslant 5.1 \times 10^4$ $\mu_N^2\mathrm{fm}^2$		
				$M1^*$		$\geqslant 0.013$ μ_N^2		
^{82}Se	$2_1^+ \to 0_1^+$		654.75(16)	$E2$	*18.9(3)* [6]	*360(6)* $e^2\mathrm{fm}^4$	295 $e^2\mathrm{fm}^4$	326 $e^2\mathrm{fm}^4$
	$4_1^+ \to 2_1^+$		1735.51(10)	$E2$	*1.38(22)* [7]	*400(60)* $e^2\mathrm{fm}^4$	417 $e^2\mathrm{fm}^4$	442 $e^2\mathrm{fm}^4$
	$6_1^+ \to 4_1^+$		1409.9(3)	$E2$	$0.56(^{+19}_{-14})$	$263(^{+88}_{-67})$ $e^2\mathrm{fm}^4$	328 $e^2\mathrm{fm}^4$	383 $e^2\mathrm{fm}^4$
	$8_1^+ \to 6_1^+$		373.5(3)	$E2$	*9522(577)* [16]	*11.9(6)* $e^2\mathrm{fm}^4$	8.1 $e^2\mathrm{fm}^4$	6.5 $e^2\mathrm{fm}^4$
	$(10_1^+) \to 8_1^+$		1940	$E2$	$\leqslant 1.5$	$\geqslant 20$ $e^2\mathrm{fm}^4$	98 $e^2\mathrm{fm}^4$	60 $e^2\mathrm{fm}^4$
					best fit: 0.4	75 $e^2\mathrm{fm}^4$		
	$2_2^+ \to 0_1^+$	100(7)	1731.5(1)	$E2$	*1.36(16)* [7]	$31(^{+7}_{-5})$ $e^2\mathrm{fm}^4$	10.7 $e^2\mathrm{fm}^4$	3.2 $e^2\mathrm{fm}^4$
	$\to 2_1^+$	26(6)	1076.4(4)	$E2^*$		$88(^{+34}_{-27})$ $e^2\mathrm{fm}^4$	64 $e^2\mathrm{fm}^4$	19 $e^2\mathrm{fm}^4$
				$M1^*$		$0.007(^{+1}_{-1})$ μ_N^2	0.0004 μ_N^2	0.065 μ_N^2
	$4_2^+ \to 2_1^+$	100(9)	1895.5(1)	$E2$	$2.4(^{+5}_{-3})$	5.7(14) $e^2\mathrm{fm}^4$	10.4 $e^2\mathrm{fm}^4$	4.7 $e^2\mathrm{fm}^4$
	$\to 2_2^+$	91(13)	818.6(2)	$E2$		$3.5(^{+1.1}_{-1.0}) \times 10^2$ $e^2\mathrm{fm}^4$	66 $e^2\mathrm{fm}^4$	109 $e^2\mathrm{fm}^4$
	$\to 4_1^+$	52(13)	815.1(2)	$E2^*$		$203(^{+87}_{-77})$ $e^2\mathrm{fm}^4$	18.9 $e^2\mathrm{fm}^4$	3.5 $e^2\mathrm{fm}^4$
				$M1^*$		0.009(4) μ_N^2	0.001 μ_N^2	0.047 μ_N^2
	$5_1^- \to 4_2^+$		343.3(3)	$E1$	$\geqslant 190$	$\leqslant 8 \times 10^{-5}$ $e^2\mathrm{fm}^2$		

$B(E2; 2_1^+ \to 0_1^+)$ and $B(E2; 4_1^+ \to 2_1^+)$ values of ^{80,82}Se were reported and discussed in previous works [6,7,12–14].

For ^{82}Se, the new experimental $B(E2; 6_1^+ \to 4_1^+)$ value is described well within the error by JUN45. In the case of ^{80}Se, the new experimental $B(E2; (6_1^+) \to 4_1^+)$ value is compatible with both calculations (see Fig. 11 and Table II).

For ^{82}Se, both calculations slightly underestimate the experimental $8_1^+ \to 6_1^+$ transition strength. A distinct difference between the calculations is visible for the $8_1^+ \to 6_1^+$ transition

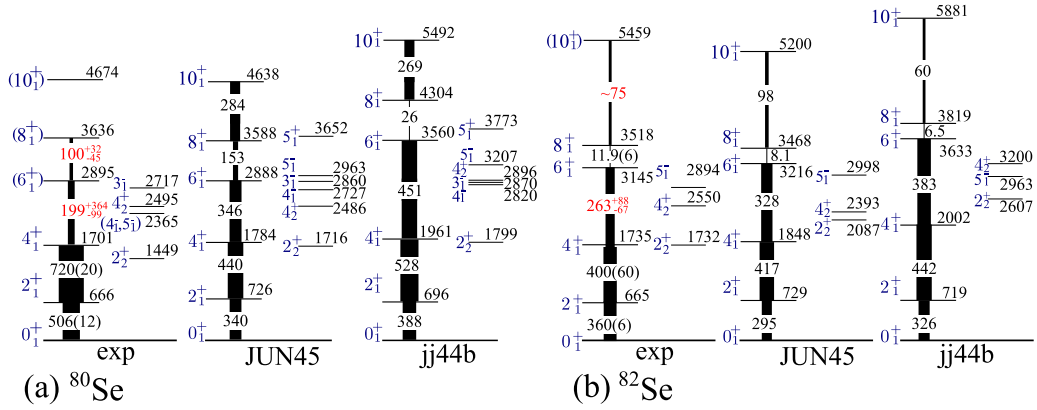

FIG. 11. Comparison of experimental and shell-model calculated 2_1^+, 4_1^+, 6_1^+, 8_1^+, and 10_1^+ yrast and 2_2^+, 4_2^+, and selected sideband excitation energies (given in keV) and, in the case of yrast states, reduced transition probabilities (given in $e^2\text{fm}^4$) of ^{80,82}Se isotopes. New experimental $B(E2)$ strengths from this work are marked red (gray).

strength in ^{80}Se, for which the JUN45 and jj44b values differ by a factor of 6. The new $B(E2;(8_1^+)\rightarrow(6_1^+))$ value is slightly overestimated by JUN45 and clearly underestimated by jj44b, which will be discussed later in this section.

For ^{82}Se, the $(10_1^+)\rightarrow 8_1^+$ transition is discussed in Sec. III B 2. From the upper lifetime limit a lower $B(E2)$ limit is calculated and, in addition, the $B(E2)$ value for the best fit is given. In both cases, shell-model calculated values for the $10_1^+\rightarrow 8_1^+$ transition probability are similar to the experimental result.

For both nuclei the 2_1^+,4_1^+,6_1^+ yrast states are interpreted to be dominated by $\pi(f_{5/2},p_{3/2})^6$ proton quadrupole-collective excitations coupled to the $\nu(g_{9/2}^{-2/-4})$ configuration [5], while the 8_1^+ states are understood to have a dominant $\nu g_{9/2}^{-2}$ configuration. This different nuclear structure leads to retarded decay transitions and often isomeric yrast 8_1^+ states for $N=48$ isotones in this region, especially in ^{82}Se with $B(E2;8_1^+\rightarrow 6_1^+)=11.9(6)\ e^2\text{fm}^4$ [16]. The corresponding transition probability in ^{80}Se is significantly larger, with $B(E2;(8_1^+)\rightarrow(6_1^+))=100(^{+32}_{-45})\ e^2\text{fm}^4$ (this work), indicating a more mixed structure for the (6_1^+) and (8_1^+) states in ^{80}Se than in ^{82}Se.

In Table III, the leading configurations of the shell-model wave functions of the yrast states up to 10_1^+ are analyzed in terms of couplings of protons and neutrons to different spins. The wave functions for ^{80,82}Se for the 0_1^+ ground state contain a notable amount of nonzero seniority configurations, i.e., $\nu 2^+\otimes\pi 2^+$ and $\nu 4^+\otimes\pi 4^+$. The calculated 2_1^+ and 4_1^+ states show a rather balanced mixture of configurations with proton and neutron character.

For both interactions, the wave functions of the 6_1^+ states in ^{80,82}Se show a mixture of mainly $\nu\otimes\pi$ configuration: $6^+\otimes 0^+$, $4^+\otimes 2^+$, and $2^+\otimes 4^+$; see Table III. In ^{82}Se, the pure proton $\nu 0^+\otimes\pi 6^+$ configuration contributes with 10.5(5.4)% for JUN45 (jj44b), which in ^{80}Se is reduced to <3% for both interactions.

The 8_1^+ states are dominated, with ≈50%, by the pure neutron $\nu 8^+\otimes\pi 0^+$ configuration for both nuclei and interactions. The main $E2$ decay of this configuration to the 6_1^+ state proceeds to the $\nu 6^+\otimes\pi 0^+$ configuration which has only ≈20%, leading to a reduced $B(E2;8_1^+\rightarrow 6_1^+)$ value for ^{80,82}Se.

TABLE III. Leading configurations built by protons and neutrons coupled to different spins in the wave functions of yrast states up to spin 10_1^+ in ^{80,82}Se resulting from shell-model calculations with JUN45 and jj44b interactions. Numbers are given in percent. Only configurations with contributions >5% for at least one interaction are listed. Further details are given in the text.

Spin	$\nu\otimes\pi$	^{80}Se		^{82}Se	
		JUN45	jj44b	JUN45	jj44b
0_1^+	$0^+\otimes 0^+$	50.8	41.1	59.0	49.8
	$2^+\otimes 2^+$	39.5	46.8	35.4	42.3
	$4^+\otimes 4^+$	6.2	8.3	4.4	6.1
2_1^+	$2^+\otimes 0^+$	27.1	25.3	26.8	26.8
	$0^+\otimes 2^+$	33.1	28.4	38.0	33.4
	$2^+\otimes 2^+$	14.1	17.0	15.2	17.0
	$4^+\otimes 2^+$	9.0	10.5	6.8	8.7
	$2^+\otimes 4^+$	9.1	9.8	9.1	9.0
4_1^+	$4^+\otimes 0^+$	19.6	17.0	13.4	16.5
	$2^+\otimes 2^+$	34.3	35.1	38.6	39.2
	$0^+\otimes 4^+$	16.1	14.4	25.1	18.6
	$4^+\otimes 2^+$	8.0	8.8	6.0	7.7
	$6^+\otimes 2^+$	5.3	5.0	2.1	2.8
	$2^+\otimes 4^+$	5.9	7.8	7.7	7.8
6_1^+	$6^+\otimes 0^+$	25.4	18.3	19.7	18.4
	$4^+\otimes 2^+$	31.1	32.6	27.6	34.5
	$2^+\otimes 4^+$	14.2	19.0	30.4	27.8
	$0^+\otimes 6^+$	2.0	2.6	10.5	5.4
	$6^+\otimes 2^+$	7.6	6.3	2.0	2.5
	$8^+\otimes 2^+$	5.6	4.0	1.1	1.2
8_1^+	$8^+\otimes 0^+$	49.1	43.6	53.4	47
	$6^+\otimes 2^+$	16.5	11.4	2.4	2.0
	$8^+\otimes 2^+$	5.6	19.4	34.5	40.6
	$10^+\otimes 2^+$	5.4	4.9		
	$7^+\otimes 2^+$	6.3	3.5		
10_1^+	$10^+\otimes 0^+$	29.8	24.1		
	$8^+\otimes 2^+$	36.2	35.6	60.2	66.9
	$8^+\otimes 4^+$	3.0	4.6	19.2	13.2
	$6^+\otimes 4^+$	8.1	8.0	13.6	7.9
	$10^+\otimes 2^+$	7.4	12.7		
	$8^+\otimes 3^+$			1.9	6.2

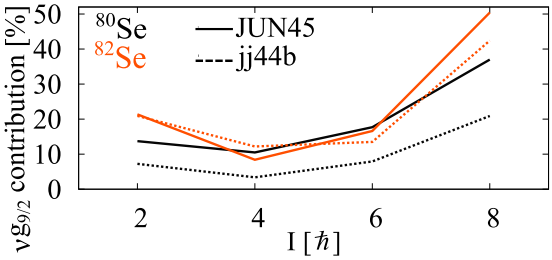

FIG. 12. Lower limit of the pure $\nu g_{9/2}$ contribution of the wave function of $2^+, 4^+, 6^+, 8^+$ states ($\nu I \otimes \pi 0^+$ configurations) in ^{80,82}Se as defined in the text.

Further on, in ^{82}Se the $\nu 8^+ \otimes \pi 2^+$ configuration forming the 8_1^+ state contributes with 34.5(40.6)% for JUN45 (jj44b), but the $\nu 6^+ \otimes \pi 2^+$ configuration of the 6_1^+ state contains only ≈2%. Thus, in ^{82}Se the decay of the dominant $\nu 8^+ \otimes \pi 0^+$ and $\nu 8^+ \otimes \pi 2^+$ configurations is hindered, leading to the very small $B(E2; 8_1^+ \rightarrow 6_1^+)$ transition strength.

For ^{80}Se, one finds a more mixed structure of the 8_1^+ state, with a clear difference between JUN45 and jj44b $E2; 8_1^+ \rightarrow 6_1^+$ strengths. Looking in more detail, in Table III the following differences between the two interactions in the main configurations can be noticed. The $\nu 8^+ \otimes \pi 0^+$ configuration for the 8_1^+ state dominates with 49.1(43.6)% for JUN45 (jj44b), whereas the $\nu 6^+ \otimes \pi 0^+$ configuration contributes with 25.4(18.3)% for the 6_1^+ state, which results in different $E2$ strengths. The second most dominant configuration of the 8_1^+ state differs for JUN45 and jj44b. As listed in Table III, in the case of JUN45 it is the $\nu 6^+ \otimes \pi 2^+$ configuration which can decay to four dominant $\nu \otimes \pi$ configurations in the 6_1^+ state, $6^+ \otimes 0^+$, $4^+ \otimes 2^+$, $6^+ \otimes 2^+$, and $8^+ \otimes 2^+$, while for jj44b it is the $\nu 8^+ \otimes \pi 2^+$ configuration which can only decay to the low percentage $\nu \otimes \pi$ configurations $6^+ \otimes 2^+$ and $8^+ \otimes 2^+$.

Another important aspect is the role of the $\nu g_{9/2}$ orbital. In order to isolate the pure $\nu g_{9/2}$ configurations coupled to $\pi 0^+$ configurations, the individual wave functions were inspected with respect to the orbital occupations and couplings, and the results are depicted in Fig. 12 for the $2_1^+, 4_1^+, 6_1^+, 8_1^+$ shell-model states. For ^{82}Se, the pure $\nu g_{9/2}$ contribution in this model space is given by the $\nu f_{5/2}^6 p_{3/2}^4 p_{1/2}^2 g_{9/2}^8$ partition and protons coupled to zero. For ^{80}Se, further configurations are possible where the neutrons in $f_{5/2}, p_{3/2}, p_{1/2}$ are not coupled to spin zero. Thus, a lower limit of the pure $\nu g_{9/2}$ configuration in the calculations can be defined by the sum of $\nu f_{5/2}^6 p_{3/2}^4 p_{1/2}^2 g_{9/2}^6$ and $\nu f_{5/2}^6 p_{3/2}^4 p_{1/2}^0 g_{9/2}^8$ partitions provided that protons are coupled to zero. As the shell-model code output [41] excludes partitions with contributions <1%, all presented numbers in Fig. 12 might miss small contributions and are therefore lower limits.

By comparing Figs. 1 and 12, it is obvious that the $B(E2)$ trends for the yrast cascades of ^{80,82}Se as calculated by JUN45 and jj44b behave approximately inversely to the $\nu g_{9/2}$ contribution of the corresponding decaying state. This is consistent with the understanding that $\nu g_{9/2}$ configurations in these nuclei are single-particle excitations, whereas the remaining percentage of the wave functions are dominantly of proton character and can be interpreted in terms of collective excitations. Figure 12 shows that for ^{80}Se one finds a higher amount of $\nu g_{9/2}$ contribution for JUN45, while for ^{82}Se the amount is nearly equal for JUN45 and jj44b except for the 8_1^+ level discussed above.

For ^{80,82}Se, the theory presented in Refs. [14,15] predicts a collective wave function up to the 6_1^+ state with approximately zero contribution of $\nu g_{9/2}^{-2}$ configurations, which is reflected in the predicted constant $E2$ strengths of the $4_1^+ \rightarrow 2_1^+$ and the $6_1^+ \rightarrow 4_1^+$ transitions (see PQM80 in Fig. 1). On the other hand, independent from the large error bar, the experimental result (this work) clearly contradicts the PQM80 calculations, indicating a decrease of $E2$ strengths for the $6^+ \rightarrow 4^+$ transition (Fig. 1). This decrease is well reproduced by calculations with the JUN45 and jj44b interactions and can be traced back to a non-negligible $\nu g_{9/2}$ contribution in the structure of the 6_1^+ state (see discussion above and Fig. 12). The truncated fpg calculations [12] have a trend similar to the PQM80 calculations, overestimating the $6_1^+ \rightarrow 4_1^+$ transition probability (see also Fig. 1).

2. *Yrare states of* ^{80,82}Se

The lowest yrare states of ^{80,82}Se show similar excitation energies as well as a similar decay pattern; see Fig. 2. In addition, their decay transition strengths are comparable, which hints at a similar structure of these states.

In the case of $\Delta I = 0$ transitions, in this case $2_2^+ \rightarrow 2_1^+$ and $4_2^+ \rightarrow 4_1^+$, multipole mixing ratios δ are necessary to calculate the $M1$ and $E2$ transition probabilities. Since for ^{82}Se these are not known, transition strengths are calculated assuming either pure $E2$ or $M1$ transitions and are listed in Table II marked with asterisks.

From Table II it is clear that on the average the $E2$ strengths are underestimated by JUN45 and jj44b, and jj44b clearly overestimates the $M1$ part of transitions from $4_2^+, 2_2^+$ yrare states in both nuclei. The only exception is the nonconfirmed $4_2^+ \rightarrow 2_2^+$ transition in ^{80}Se, whose $E2$ strength is clearly overestimated by both calculations. However, to understand the structure of these states, further experimental and theoretical investigations are necessary.

3. *Sideband in* ^{80}Se

In ^{80}Se, transitions were experimentally identified and assigned as a sideband on top of the yrast 4_1^+ state [5]. In this work, lifetime information is gained for three band members; see 2365-keV, 2784-keV, and 3364-keV levels in Fig. 2(a) and also Table II. In order to discuss the possible type and multipolarity of the transitions in this sideband, $B(\sigma\lambda)$ values were calculated under the assumptions of pure $E1$, $E2$, $M1$, or $M2$ transitions, respectively, and are listed in Table II marked with asterisks.

For the 2365-keV level, spins $I < 2$ and $I > 6$ independent from the parity would result in transitions with multipolarities $\geqslant 3$, which can be excluded. From Table II it is clear that $M2$ transitions are unrealistic due to the resulting transition probability of 1972, 15 610 W.u., therefore 2^- and 6^- states can be excluded, too. The 2365-keV level solely decays to the yrast 4_1^+ state via $E_\gamma = 664$ keV. Therefore, positive parity levels with spins $I \leqslant 4\hbar$ can be generally ruled out, as in

these cases a transition to the ground state or the 2_1^+ state would most probably have a non-negligible branch which should have been experimentally observed. The decay patterns of JUN45 and jj44b calculated low-spin positive-parity states were inspected for levels with dominant decay branches to the 4_1^+ state, and all show in addition a non-negligible decay branch to the lower-lying yrast states. The same argument also holds for a possible 3^- assignment, which therefore can also be excluded. Furthermore, a 3^- state is experimentally known at an excitation energy of 2717 keV, which mainly decays to the yrast 2_1^+ state. This 3_1^- state is described well by JUN45 and jj44b; see Fig. 11. This leaves possibilities of 4^-, 5^-, 5^+, and 6^+ for the 2365-keV level.

Assuming the 2365-keV level is the yrast 6_1^+ state and, consequently, the band on top of it is the further yrast band, neither fits the systematics compared to neighbor nuclei, especially ^{82}Se, nor the presented shell-model calculations for ^{80}Se. At excitation energies around 3 MeV, the yrast (6_1^+) state as well as an yrare (6_2^+) state for ^{80}Se were experimentally identified [42,43]. Both 6^+ states and the whole yrast sequence of ^{80}Se including the (6_1^+) state are well reproduced by JUN45 and jj44b. Therefore, we also exclude an $I^\pi = 6_1^+$ assignment for the 2365-keV level.

The shell-model calculations also predict two 5^+ states above 3.5 MeV, with the lower one shown in Fig. 11. Including the $\nu d_{5/2}$ orbital in the shell-model space, one would expect a shift of the calculated 5_1^+ level to lower energies, especially pronounced approaching $N = 50$. In the closed-shell nucleus ^{84}Se a 5^+ state based on the $\nu g_{9/2}^{-1} d_{5/2}^{+1}$ configuration [1,18] is known at 3537 keV [23], while JUN45 predicts the 5_1^+ state at 3849 keV. Therefore, it seems unlikely that, even including the $\nu d_{5/2}$ orbital, the calculated 5^+ states in ^{80}Se would be shifted down to energies below 2.5 MeV, and thus it is unlikely that the 2365-keV level is of 5^+ character.

Experimental information on 4^- and 5^- states in neighboring even-even nuclei around ^{80}Se is summarized in Table IV. Following the systematics of neighboring even-even nuclei, one expects a 5^- state around 2600–3000 keV excitation energy, mainly decaying to a 4^+ state (Table IV) and with a level lifetime in the picoseconds range [23]. In ^{80}Se the lowest 5^- state observed so far is at $E = 3996$ keV excitation energy [44]. The 2365-keV level is lower in excitation energy compared to the 5^- of direct even-even neighbors; see Table IV. Similar to 5^-, a 4^- assignment is possible, but 4^- states in the neighboring nuclei also occur higher in energy. In analogy to the neighboring isotopes in ^{80}Se, a decay branch of the 4_1^- level to the 3_1^+ state at 2121.1 keV would be expected. However, the energy difference between the 2365-keV level and the 3_1^+ state is small, $\Delta E = 244$ keV, and thus this branch might be suppressed compared to the 664-keV transition to the 4_1^+ state. A $4^- \to 4_1^+$ as well as a $5^- \to 4_1^+$ decay would be of $E1$ character. From the lifetime a $B(E1;(4^-,5^-) \to 4_1^+) =$ 0.0015–0.0002 W.u. value results, which is consistent with the recommended upper limit for an $E1$ transition in $A = 45 - 90$ nuclei [45].

From the shell-model point of view, JUN45 and jj44b predict several negative-parity states around 3 MeV, among them a 4^- and a 5^- state (see Fig. 11), and their wave functions have a dominant configuration of neutrons $f_{5/2}^6 p_{3/2}^4 p_{1/2}^1 g_{9/2}^7$ coupled to $I^\pi = 4^-,5^-$ and protons with configurations coupled to $I^\pi = 0^+,2^+$. This corresponds simply to an excitation of a neutron from the $p_{1/2}$ to the $g_{9/2}$ orbital. Thus, any change in the relative position of the orbitals, i.e., single-particle energies, will change the energy of the calculated 4^- and 5^- states in the shell-model spectra.

For the 2784-keV level, a lower lifetime limit is derived which leads to upper limits for the transition probabilities. From these it becomes clear that an $E1$, $E2$, $M1$, or $M2$ transition is possible, which leads to possible spins $2 \leqslant I \leqslant 7$ for the 2784-keV level, assuming a spin of $I = 4,5$ for the band head. The shell-model calculations predict numerous levels with such spins in the range of 3–4 MeV, but no further conclusion on the spin and parity can be done reliably. In case of the 3364-keV level an $M2$ decay can be ruled out, leaving $E1$, $E2$, or $M1$ transitions possible, but again no spin-parity assignment can be suggested.

V. SUMMARY AND CONCLUSION

In summary, lifetimes of intermediate-spin yrast states in ^{80,82}Se as well as yrare and sideband level lifetimes were measured in a recoil distance Doppler-shift experiment. Transition

TABLE IV. Summarized experimental information for the lowest observed 5^- and 4^- states [23] in the neighboring even-even nuclei. Only the dominating decay branch is listed. The corresponding information for ^{80}Se is given in italics under the assumption that the 2365-keV state is of (5_1^-) or (4_1^-) character.

	N	44	46	48	44	46	48
$_{36}$Kr	E (keV)	2859.53	2828	2770.9	2793	2648.4	4001.82(11)
	$I_i \to I_f$	$5_1^- \to 4_1^+$	$(5_1^-) \to 4_1^+$	$5_1^- \to 4_2^+$	$4_1^- \to 3_1^+$	$4_1^- \to 3_1^+$	$(4_1^-) \to 5_1^-$
	$B(E1)$ (10^{-3} e^2fm^2)	0.06(3)	0.03(2)	0.74(2)		≈0.2	>0.38
	$B(M1)$ (μ_N^2)						0.03(1)
$_{34}$Se	E (keV)	2889.9	*2365*	2893	2742	*2365*	
	$I_i \to I_f$	$5_1^- \to 4_1^+$	$(4_1^-,5_1^-) \to 4_1^+$	$5_1^- \to 4_2^+$	$4_1^- \to 4_2^+$	$(4_1^-,5_1^-) \to 4_1^+$	
	$B(E1)$ (10^{-3} e^2fm^2)	0.010(3)	*1.8–0.23*	⩽0.08	≈0.01	*1.8–0.23*	
$_{32}$Ge	E (keV)	2957.9(15)	2652				
	I_i	5_1^-	(5_1^-)				

strengths from these new level lifetimes were calculated which complete the picture of $E2$ strengths for ^{80,82}Se up to the $8_1^+ \rightarrow 6_1^+$ transition and enable to probe nuclear models for yrast, yrare, and other sideband levels.

Shell-model calculations using the effective interactions JUN45 and jj44b were presented and discussed, including the role of the neutron $g_{9/2}$ orbital. The transition between the rotational (mid-shell) region and the single particle (closed shell) region at $N = 50$ in selenium isotopes is particularly obvious when following $B(E2)$ trends of the corresponding yrast bands. As shown, the change of nuclear structure induced by the filling of the neutron $g_{9/2}$ orbital already happens in ^{80}Se, and neutron $g_{9/2}^{-2/-4}$ configurations are essential for the description not only of the 8_1^+ state but also of the 6_1^+ state, contrary to the theoretical predictions from Refs. [14,15]. The predicted reduction of the $B(E2, 8_1^+ \rightarrow 6_1^+)$ values from ^{78}Se towards ^{80,82}Se [12,14,15] is confirmed by this measurement. For ^{80,82}Se, the new experimental $6_1^+ \rightarrow 4_1^+$ transition strengths are smaller than those theoretically predicted by fpg and PQM80; see Fig. 1. Despite the large uncertainties, shell-model calculations with the JUN45 interaction succeed best in describing the yrast $B(E2)$ trends up to the 8_1^+ states both for ^{80}Se and ^{82}Se, although it should be noted here that experimental values do not allow us to distinguish within 3σ between the different shell-model calculations.

Concerning yrare states in ^{80,82}Se, the comparison of experimental transition strengths with JUN45 and jj44b calculated values points out deficiencies in the description of transition strengths from the 2_2^+ and 4_2^+ states.

The head of a sideband in ^{80}Se with $E^* = 2365$ keV is suggested to be the lowest (5^-) or (4^-) state, based on the $E1$ transition strengths, the comparison with neighboring nuclei, and shell-model calculations.

ACKNOWLEDGMENTS

This work was partially supported by the European Union Seventh Framework Program FP7/2007-2013 under Grant Agreement No. 262010 ENSAR, by the German Research Foundation (DFG) under Contract No. DE 1516/3-1, by the German BMBF under Grant No. 05P15PKFNA and by the Spanish Ministerio de Economía y Competitividad under Contract No. FPA2014-57196-C5-4-P. J.L. and A.V. thank the Bonn-Cologne Graduate School of Physics and Astronomy (BCGS) for financial support.

[1] A. Prévost *et al.*, Eur. Phys. J. A **22**, 391 (2004).
[2] F. Drouet *et al.*, EPJ Web Conf. **62**, 01005 (2013).
[3] E. F. Jones *et al.*, Phys. Rev. C **73**, 017301 (2006).
[4] Y. H. Zhang *et al.*, Phys. Rev. C **70**, 024301 (2004).
[5] G. A. Jones *et al.*, Phys. Rev. C **76**, 054317 (2007).
[6] R. Lecomte *et al.*, Nucl. Phys. A **284**, 123 (1977).
[7] J. Barrette, M. Barrette, G. Lamoureux, S. Monaro, and S. Markiza, Nucl. Phys. A **235**, 154 (1974).
[8] S. Raman *et al.*, At. Data Nucl. Data Tables **78**, 1 (2001).
[9] M. G. Porquet *et al.*, Eur. Phys. J. A **39**, 295 (2009).
[10] A. Gade *et al.*, Phys. Rev. C **81**, 064326 (2010).
[11] J. Litzinger *et al.*, Phys. Rev. C **92**, 064322 (2015).
[12] P. C. Srivastava and M. J. Ermamatov, Phys. Scr. **88**, 045201 (2013).
[13] K. Nomura, R. Rodríguez-Guzmán, and L. M. Robledo, Phys. Rev. C **95**, 064310 (2017).
[14] N. Yoshinaga, K. Higashiyama, and P. H. Regan, Phys. Rev. C **78**, 044320 (2008).
[15] N. Yoshinaga and K. Higashiyama, J. Phys.: Conf. Ser. **445**, 012032 (2013).
[16] A. Makishima, M. Asai, T. Ishii, I. Hossain, M. Ogawa, S. Ichikawa, and M. Ishii, Phys. Rev. C **59**, R2331(R) (1999).
[17] Yu. G. Kosyak, L. V. Chekushina, Zh. I. Adymov, A. S. Ermatov, and G. A. Urikbaeva, Bull. Rus. Acad. Sci. Phys. **63**, 110 (1999).
[18] G. Winter *et al.*, Phys. Rev. C **48**, 1010 (1993).
[19] M. Honma, T. Otsuka, T. Mizusaki, and M. Hjorth-Jensen, Phys. Rev. C **80**, 064323 (2009).
[20] D. Verney *et al.* (PARRNe Collaboration), Phys. Rev. C **76**, 054312 (2007).
[21] B. Cheal *et al.*, Phys. Rev. Lett. **104**, 252502 (2010).
[22] O. Sorlin *et al.*, Phys. Rev. Lett. **88**, 092501 (2002).
[23] Brookhaven National Nuclear Data Center, http://www.nndc.bnl.gov.
[24] A. Dewald, O. Möller, and P. Petkov, Prog. Part. Nucl. Phys. **67**, 786 (2012).
[25] D. Montanari, Ph.D. thesis, University of Milan, Italy, 2009 (unpublished).
[26] A. Stefanini *et al.*, Nucl. Phys. A **701**, 217 (2002).
[27] S. Szilner *et al.*, Phys. Rev. C **76**, 024604 (2007).
[28] L. Corradi *et al.*, Nucl. Instrum. Methods Phys. Res., Sect. B **317**, 743 (2013).
[29] S. Akkoyun *et al.*, Nucl. Instrum. Methods Phys. Res., Sect. A **668**, 26 (2012).
[30] A. Gadea *et al.*, Nucl. Instrum. Methods Phys. Res., Sect. A **654**, 88 (2011).
[31] B. Bruyneel, B. Birkenbach, and P. Reiter, Eur. Phys. J. A **52**, 70 (2016).
[32] A. Lopez-Martens, K. Hauschild, A. Korichi, J. Roccaz, and J.-P. Thibaud, Nucl. Instrum. Methods Phys. Res., Sect. A **533**, 454 (2004).
[33] A. B. Brown, C. W. Snyder, W. A. Fowler, and C. C. Lauritsen, Phys. Rev. **82**, 159 (1951).
[34] K.-H. Speidel *et al.*, Phys. Rev. C **57**, 2181 (1998).
[35] S. Agostinelli *et al.*, Nucl. Instrum. Methods Phys. Res., Sect. A **506**, 250 (2003).
[36] D. Mengoni, J. J. Valiente-Dobón, E. Farnea, A. Gadea, A. Dewald, and A. Latina, Eur. Phys. J. A **42**, 387 (2009).
[37] J. J. Valiente-Dobón *et al.*, Phys. Rev. Lett. **102**, 242502 (2009).
[38] L. Corradi, G. Pollarolo, and S. Szilner, J. Phys. G **36**, 113101 (2009).
[39] A. Vogt *et al.*, Phys. Rev. C **92**, 024619 (2015).
[40] O. Tarasov and D. Bazin, Nucl. Instrum. Methods Phys. Res., Sect. B **204**, 174 (2003).
[41] B. Brown and W. Rae, Nucl. Data Sheets **120**, 115 (2014).

[42] M. G. Porquet *et al.*, in *The Second International Workshop on Nuclear Fission and Fission-Product Spectroscopy*, April 1998, Seyssins, France, edited by G. Fiono, H. Faust, S. Oberstedt, and F.-J. Hambsch, AIP Conf. Proc. No. 447 (AIP, New York, 1998), p. 212.

[43] M. Burlein, H. T. Fortune, D. L. Watson, and M. D. Cohler, Phys. Rev. C **34**, 1592 (1986).

[44] K. Ogino, Phys. Rev. C **33**, 71 (1986).

[45] P. Endt, At. Data Nucl. Data Tables **23**, 547 (1979).